Controlled mobility of compact discrete solitons in nonlinear Lieb photonic lattices

Bastián Real and Rodrigo A. Vicencio
Departamento de Física and Millennium Institute for Research in Optics (MIRO), Facultad de Ciencias and Facultad de Ciencias Físicas y Matemáticas, Universidad de Chile, Santiago, Chile

(Received 3 August 2018; published 26 November 2018)

We study the mobility of localized solutions in a nonlinear Lieb photonic lattice. We characterize different families of nonlinear solutions looking for different regions of parameters to observe coherent transport across the system. In particular, we analytically derive a family of compact discrete solitons, which originate at the flat band of this lattice at zero power. For low level of power, we found a transparent region where two well-localized nonlinear modes, which are close in Hamiltonian, show a very good mobility. We numerically observe a perfect transport across the system with negligible radiation, where two compact solutions adiabatically transform one into the other. Although the ring mode stabilizes for larger power, it is not parametrically connected to any other stationary solution and, therefore, it is not allowed to move across the system for high power.

DOI: 10.1103/PhysRevA.98.053845

I. INTRODUCTION

For several decades, researchers have been interested on finding the right conditions to observe localization and mobility across a given lattice [1–3]. The problem essentially consisted on defining a lattice geometry and looking for stationary solutions at the bulk or surfaces, considering different nonlinearities and/or effective linear interactions. Many theoretical and experimental observations were performed and the conditions for controlling the energy on a discrete nonlinear system are nowadays well understood, although good discrete mobility has been experimentally elusive so far.

Recently, a new interesting topic started to be explored deeply, the one considering nonconventional lattice geometries. Specifically, it was found that for some specific lattices a nonstandard linear spectrum appears, which includes at least one or even more zero-dispersion bands [4–8]. This unusual linear spectrum allows the existence of completely linear localized profiles, which somehow solved trivially the problem of localizing energy on a given discrete system [9]. In fact, these localized states occupy only few lattice sites, they are completely stable, and they can be linearly superposed to form complex patterns at will [10–13]. Additionally, they exist for powers and energies as low as the detection level of the devices used to measure them. All these properties are crucial when trying to effectively apply the discrete lattice phenomena into concrete photonic applications [14].

On the other hand, coherent transport in two-dimensional (2D) nonlinear discrete systems has been proposed to occur in different lattice geometries [2,3]. However, most of these predictions have been performed at low level of power, where localized solutions are broader and spatially similar to wide Gaussian profiles. At this regime the Hamiltonian differences between fundamental stationary solutions are very small [15] and, therefore, the Peierls-Nabarro (PN) barrier is easily overcome by a simple phase gradient [16,17]. Alternatively, the mobility of high power and well-localized solutions has been also showed in saturablelike systems [18–22]. A nonlinear saturation mechanism is necessary in order to obtain a simultaneous increment of the peak amplitude and the solutions width. This is important to reduce the Hamiltonian differences and, consequently, the effective PN barrier, which finally facilitates the mobility of localized excitations.

The mobility at low level of power and for highly localized solutions is not allowed in standard geometries. However, it was recently shown [23] that the existence of a flat band (FB) at the bottom of the linear spectrum made possible a very interesting stability exchange mechanism. For a nonlinear kagome lattice, a ring FB mode bifurcates at the FB frequency at zero power. When considering a defocusing nonlinearity, the FB mode evolves directly into the gap, being initially stable and having a participation ratio of only six sites. A one-peak solution can be constructed by linearly superposing two ring modes, which bifurcate exactly at the FB energy (this is completely different to the standard bifurcation mechanism where one-peak solutions bifurcate from an extended linear mode at the edge of the linear spectrum). This solution has initially a participation ratio larger than 6 and, as a consequence, occupies a larger area and possesses a larger Hamiltonian, being therefore unstable. As the ring mode preserves its area for any level of power, there must be a stability exchange between these two solutions because the one-peak state rapidly decreases its participation ratio for an increasing power (being, in fact, just one for an infinite norm). Even though it was shown that for kagome lattices good mobility is possible, other FB lattices have not showed the same phenomenology. For example, a nonlinear kagome ribbon [24] or a dimerized Lieb lattice [25] has showed no effective transport at all.

In this work, we study the dynamical properties of an homogeneous nonlinear Lieb photonic lattice. We focus on the identification of the main properties of a defined set of fundamental nonlinear stationary solutions. We look for conditions to observe multistability regimes that could open a dynamical window of good transport in the parameter space.

For low level of power, we find very good transport as a consequence of a smooth transformation between single-peak and ring discrete solitons. We observe an stabilization of the FB nonlinear mode for larger powers, but no connection of this solution with any other fundamental mode implying, as a consequence, no transport at high energy.

II. MODEL

We model the propagation of light in a weakly coupled system using a set of discrete nonlinear Schrödinger (DNLS) equations with Kerr-type nonlinearity. We assume a Lieb geometry and describe the light evolution on this lattice by using the following set of coupled equations [2,3]:

$$-i\frac{d\psi_{\vec{n}}}{dz} = \beta_{\vec{n}}\psi_{\vec{n}} + \sum_{\vec{m}\neq\vec{n}} V_{\vec{n},\vec{m}}\psi_{\vec{m}} + \gamma|\psi_{\vec{n}}|^2\psi_{\vec{n}}. \quad (1)$$

Here, z is the propagation coordinate or dynamical variable, which in other contexts corresponds to time. $\beta_{\vec{n}}$ corresponds to the propagation constant at the $\vec{n}$th site, and for an homogeneous lattice we simply set $\beta_{\vec{n}} = 0$, without loss of generality. We define the lattice geometry through the definition of the coupling interaction $V_{\vec{n},\vec{m}}$ between sites $\vec{n}$ and $\vec{m}$ of the lattice, considering the geometry sketched in Fig. 1(a). γ corresponds to the nonlinear cubic coefficient, and its sign defines the focusing (positive) and defocusing (negative) cases. Model (1) possesses two conserved quantities, the power (or norm)

$$P \equiv \sum_{\vec{n}} |\psi_{\vec{n}}|^2, \quad (2)$$

and the Hamiltonian (or energy)

$$H \equiv -\sum_{\vec{n}}\left[\left(\sum_{\vec{m}\neq\vec{n}} V_{\vec{n},\vec{m}}\psi_{\vec{m}}\psi^*_{\vec{n}} + \text{c.c.}\right) + \frac{\gamma|\psi_{\vec{n}}|^4}{2}\right]. \quad (3)$$

We use these fundamental quantities to classify different solutions as well as to check the accuracy of our numerical simulations.

In general, the linear properties of any periodical system are contained in the definition of $V_{\vec{n},\vec{m}}$ coefficients, which describe the linear interactions between different lattice sites. We solve the linear stationary problem ($\gamma = 0$) by using a plane-wave (Bloch) ansatz of the form

$$\psi_{\vec{n}}(z) = \phi_{\vec{n}} e^{i\vec{k}\cdot\vec{n}} e^{ik_z z}.$$

Here, $\vec{k} \equiv \{k_x, k_y\}$ represents the propagation vector in the transversal plane, and k_z the longitudinal propagation constant (along the text, we will also call it frequency [3]). By inserting this ansatz into model (1), we obtain the following set of coupled stationary equations

$$k_z(\vec{k})\phi_{\vec{n}} = \sum_{m\neq n} V_{\vec{n},\vec{m}}\phi_{\vec{m}}\, e^{i\vec{k}\cdot(\vec{m}-\vec{n})}. \quad (4)$$

The number of sites per unitary cell defines the number of different amplitudes $\phi_{\vec{n}}$ to be considered in order to solve (4). Our system has three sites per unitary cell [sites A, B, and C, as shown in Fig. 1(a)] and, therefore, we will require only three different amplitudes to completely characterize the linear properties of our system. By solving the eigenvalue problem (4), we obtain the linear spectrum or band structure of a homogeneous Lieb lattice

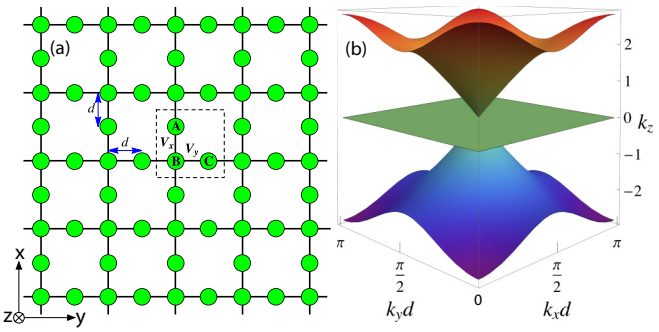

FIG. 1. (a) A Lieb photonic lattice, where the unitary cell is composed of three sites: A, B, and C. (b) Linear spectrum of an isotropic and homogeneous Lieb lattice: $V_x = V_y = 1$.

$$k_z(k_x, k_y) = 0,\ \pm 2\sqrt{V_x^2\cos^2(k_x d) + V_y^2\cos^2(k_y d)}. \quad (5)$$

Two dispersive bands are found in this system (showing a particle-hole symmetry [26]), which are connected at $k_z = 0$ by one Dirac cone located at the center of the first Brillouin zone. Additionally, at $k_z = 0$ a complete zero-dispersion flat band is found, which is one of the main linear properties of this lattice. Figure 1(b) shows the three linear bands considering an isotropic system ($V_x = V_y$). The flat band, whose group velocity and diffraction coefficient are identically zero, implies the existence of completely localized states which do not diffract upon propagation [8,9,11,27]. Modes belonging to this FB satisfy the condition $A = -C$ and $B = 0$, for an isotropic lattice system [8,28].

III. NONLINEAR LOCALIZED SOLUTIONS

Now, we look for nonlinear stationary solutions using an ansatz similar to the previous one: $\psi_{\vec{n}}(z) = \psi_{\vec{n}}\exp(-ik_z z)$, where $\psi_{\vec{n}}$ and k_z correspond to the amplitude profile and the nonlinear propagation constant (frequency), respectively. We look for real solutions ($\psi_{\vec{n}} \in \mathbb{R}$) and by inserting the ansatz into model (1), we get

$$k_z\psi_{\vec{n}} = \sum_{\vec{m}\neq\vec{n}} V_{\vec{n},\vec{m}}\psi_{\vec{m}} + \gamma\psi^3_{\vec{n}}. \quad (6)$$

Due to the symmetry of the linear spectrum, any localized nonlinear solution obtained with defocusing nonlinearity has a counterpart in the focusing regime, excepting a trivial phase transformation [2,3]. This means that the sign of the nonlinearity does not play a fundamental role on the profile of localized solutions. Therefore, without loss of generality, we simply set $\gamma < 0$ (defocusing nonlinearity). Along this work, we will also assume an isotropic ($V_x = V_y$) and a homogeneous ($\beta_{\vec{n}} = 0$) Lieb lattice.

First of all, we study the nonlinear continuation of fundamental localized flat band states; i.e., a four-sites profile with $B = 0$ and $A = -C$ [8,11,27]. After inserting this profile into

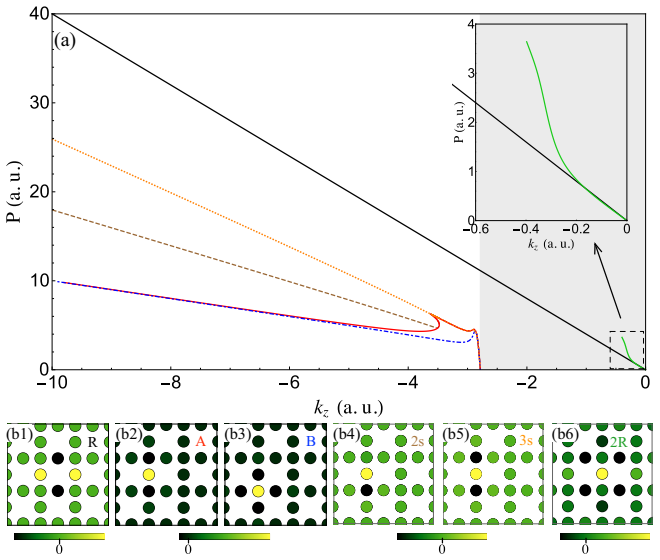

FIG. 2. (a) P versus k_z diagram for the following modes: (b1) R mode, (b2) A mode, (b3) B mode, (b4) $2s$ mode, (b5) $3s$ mode, and (b6) $2R$ mode, represented by black, red (gray), blue (dot-dashed), brown (dashed), orange (dotted), and green (light-gray) lines, respectively. The shaded area in (a) shows half of the linear band. Inset in (a): zoom at low power.

Eq. (6), we obtain the analytical solution

$$k_z = \gamma A^2 \Longrightarrow P = \frac{4k_z}{\gamma} \quad \text{and} \quad H = -\frac{\gamma P^2}{8},$$

with $P = 4A^2$ for this localized solution. Consequently, the flat band profile is also an exact stationary solution in the nonlinear regime. As this solution corresponds to a perfectly localized nonlinear mode, without any tail, it can be classified as a perfect compacton solution [29–31]. The frequency of this state grows linearly with power as plotted in Fig. 2(a) (see black straight line), having the four-sites profile showed in Fig. 2(b1). Since this nonlinear solution does not correspond to a linear FB state, we called it simply R mode due to its ringlike structure [32].

To numerically compute standard nonanalytical nonlinear stationary solutions, we consider a Lieb photonic lattice composed of 225 waveguides, with fixed boundary conditions. We implement a multidimensional Newton-Raphson iterative method to solve model (6), considering two different cases: one controlling the frequency k_z and one controlling the power P. By varying the frequency, we look for solutions with different geometry and we construct the corresponding power versus frequency diagrams. Specifically, we first look for the main fundamental solution of any nonlinear discrete system, the so-called one-site solution (also known as odd mode). This state corresponds to the geometrically simplest fundamental nonlinear discrete mode, which bifurcates from an extended linear state at the band edge [33]. For larger powers it transforms into a very localized entity, which helps us to find it numerically in the so-called anticontinuous limit [2,3]. We construct two different families of one-site solutions: the A and B modes, which depend on the number of nearest neighbors (in the isotropic case, a one-peak solution at site C is completely equivalent to the one at site A). Red (gray) and blue (dot-dashed) curves in Fig. 2(a) show the dependence of these two solutions, respectively, while Figs. 2(b2) and 2(b3) show their profiles at $k_z = -10$. The B mode follows a standard 2D dependence [33], including a direct bifurcation from a staggered band-edge mode at $k_z \approx -2.8$, which is expected due to the simpler geometry of this nonlinear solution. However, the A mode possesses a different evolution. It separates from the B mode around $k_z \approx -5$ and it gains power faster while increasing its frequency. After a frequency threshold around $k_z \approx -3.5$, it continues the increment of its power but now by decreasing its frequency up to a point where it finally fuses with a three-sites solution [orange (dotted) curve in Fig. 2(a)].

In order to understand the dynamical connection between A and B states, we look for another nonlinear solution having similar amplitudes at sites A and B. This solution is showed in Fig. 2(a) by a brown (dashed) curve and its profile at $k_z = -10$ is showed in Fig. 2(b4) [for an isotropic lattice, this solution can be excited in any pair of neighbor sites]. In standard lattices, this state is called a two-sites solution or even mode, and we call it here a $2s$ state. For a Lieb lattice, this solution is asymmetric for a decreasing value of power due to the different connections experienced by A and B sites. In fact, this mode is closer to an intermediate state of saturablelike models [18–22], which corresponds to a state that dynamically connects two fundamental solutions, which share stability properties. In the context of a Lieb lattice, it is important to find the possible dynamical connection between A, B and $2s$ solutions as we will describe below. As we observe in Fig. 2(a), the $2s$ mode monotonously decreases its power up to drastically converging to the A mode curve. This means that this solution transforms into a broader profile, while increasing its frequency. In fact, it becomes identical to the A-mode profile at the connecting point around $k_z \approx -3.5$.

Additionally, we explore another type of solution, which possesses three sites on a row, of similar amplitude and with a staggered phase structure, which we call a $3s$ solution [see Fig. 2(b5), also for $k_z = -10$]. The diagram for this mode is showed in Fig. 2(a) by an orange (dotted) curve. We observe that the $3s$ solution monotonously decreases its power while its frequency increases. Around $k_z \approx -3.6$, this solution fuses with the A mode. Then, it continues decreasing its power following a standard 2D behavior, including a power threshold close to $k_z \approx -3$. Finally, it connects to the bifurcating branch originated at the band edge (similar to the B-mode dependence, but having a larger norm).

The last nonlinear solution we consider in our analysis exactly bifurcates at the flat band frequency. This solution is formed as a linear combination of two linear FB modes (horizontally oriented in this case). To find this solution, we use an iterative method, which varies the power in order to construct a family of, what we call, $2R$ solutions, as shown in Fig. 2(a) by a green (light-gray) curve. The profile of this mode at $P = 0.001$ is presented in Fig. 2(b6). The $2R$ solution exists only in a small region inside the band, and it rapidly diverges in power due to a rapidly increasing background or tail. This is a direct manifestation of resonances with the linear spectrum, which is usually responsible of an abrupt increment of power [21,34]. This also implies a rapid reduction of the

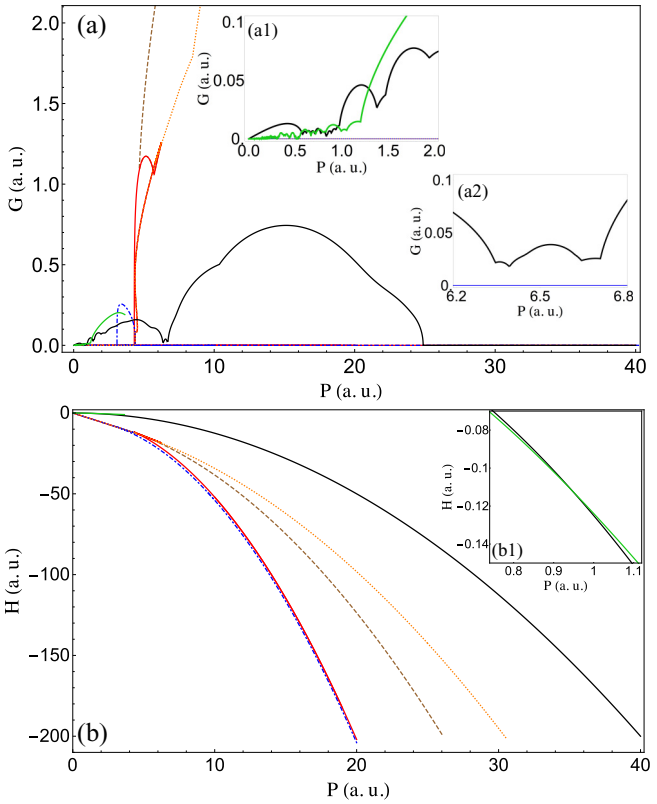

FIG. 3. (a) G-P and (b) H-P diagrams. (a1) zoom at low power and (a2) zoom at $P \sim 6.5$. (b1) zoom at $P \sim 0.95$. Colors indicate the same solutions showed in Fig. 2(a).

convergency of our iterative method, which suddenly stops the numerical continuation. It is important to mention that the R and the $2R$ modes bifurcate from the FB at zero level of power. This picture is similar to what was predicted for a nonlinear kagome lattice [23], and it is completely different to the standard bifurcation phenomenology of 2D nonlinear discrete systems [2,3,33].

In order to understand deeply the main properties of these six nonlinear stationary solutions, we implement a linear stability analysis by following a standard method [35]. We linearly perturb the nonlinear solutions and obtain a set of equations for the perturbation, which yields to a linear eigenvalue spectrum. We look for the largest eigenvalue G, which indicates the most unstable perturbation mode and, hence, the degree of linear instability of a given solution (perturbation modes start to grow on a distance $z \sim 1/G$). Therefore, in our analysis, stable and unstable nonlinear modes correspond to $G = 0$ and $G \neq 0$, respectively. Fig. 3(a) shows a G versus P diagram for all the nonlinear solutions described above.

The R and $2R$ solutions show an interesting stability evolution for low level of power [see Fig. 3(a1)]. Once the R solution becomes nonlinear (for $|k_z| > 0$), it immediately develops a weak destabilization process due to resonances with extended waves inside the linear band. The $2R$ mode is essentially stable, with only weak fluctuations very close to $G = 0$. Then, there is a region where both solutions become simultaneously weakly unstable around $P \approx 0.75$. Afterward, the $2R$ mode becomes more unstable than the R state, and close to $P \approx 3.7$ this mode is not continued anymore due to the lack of convergency. For larger powers the R solution tends to stabilize again, but it does not become completely stable as showed in Fig. 3(a2). In fact, this region looks promising as well to observe coherent transport across the lattice, as a possible multistable region. Over this level of power, the R solution becomes even more unstable achieving its maximum instability close to the region where its frequency is close to the band edge. Then, its coefficient G decreases as a manifestation of a predominant linear localized perturbation, which starts to resonate strongly with the R-mode profile. The R instability goes finally to zero at $P \approx 25$, where the main localized linear perturbation coincides with the solution profile. Again, this stabilization process could be a good indication of a multistable regime, which has been shown to be a good scenario for nonlinear discrete mobility [18–23].

Solutions A, B, $2s$, and $3s$ are stable for a low-power regime, where they fuse and become indistinguishable. While the power increases, the $2s$ and $3s$ solutions become highly unstable with a divergent G curve [see Fig. 3(a) for $P \gtrsim 4$]. A and B single-peak solutions are unstable in their power threshold regions, where the curvature in P-k_z space changes and the stability follows a standard Vakhitov-Kolokolov criterion [36]. However, both solutions become linearly stable again when P-k_z curves change their slopes again. They remain completely stable for higher level of power with $G = 0$ for $P \gtrsim 4$ (3) for the A (B) mode [both one-peak solutions transform into the ground state of the system, at different generic lattice positions, as Fig. 2(a) shows].

One additional quantity to be analyzed in DNLS-like systems is the Hamiltonian H. In Fig. 3(b), we observe the Hamiltonian versus power diagram for all the solutions found. H gives us a good indication about the possible transversal mobility of a given solution, when this nonlinear mode is compared to another stationary solution. In Fig. 3(b1) we observe a clear crossing of Hamiltonians between the R and $2R$ solutions, which occurs for low level of power. For $P \lesssim 1$, the $2R$ mode has a smaller Hamiltonian compared to the R solution, being effectively more stable as predicted in Fig. 3(a1). Afterward, both solutions share (weak) instability, their Hamiltonian cross each other at $P \approx 0.95$, and then the R mode becomes a solution having a smaller H value, being also less unstable than the $2R$ mode. Consequently, this region becomes an interesting scenario in which to study a possible coherent mobility between these two modes, because the PN barrier [16] becomes very small and solutions remain quite localized in space.

In general, the ground state of the system will be the one having the smaller H value, for a given power P. As H is determined by linear and nonlinear interactions, a solution with more connections (broader profile) will generally have a larger H value and, hence, will be unstable compared to a more localized solution. In this sense, a ring mode possesses a larger H value compared to both one-peak (A and B) solutions. Additionally, although the B mode has four main nearest neighbors, its excited area occupies a smaller region compared to the one of an A mode; therefore, $H_B < H_A$ as showed in Fig. 3(b) [the blue (dot-dashed) curve is always bellow the red (gray) one]. In general, we observe that A, B, $2s$, and $3s$ solutions exist in a region far away in Hamiltonian

from the R and $2R$ modes, without any possibility of crossing in the whole space of parameters. As a consequence, the possible mobility regimes commented above, when finding multistability regions for $P \sim 6.5$ or $P \sim 25$, are not really possible for this lattice due to the large effective energy barriers. Although for larger power A, B, and R modes are simultaneously stable, they are not dynamically connected and no mobility will be observed between these solutions. There is also a possibility to observe mobility between A and B modes, passing through a $2s$ unstable state. However, as we see in Fig. 3(b), the differences in Hamiltonian are very large between these modes. There is also an interesting region close to the connecting point ($P \sim 4$), but in this region the solutions are broader and no localized mobility can be observed. Additionally, the $2s$ solution is highly unstable in this region. Therefore, any attempt to pass through it by, for example, kicking an A or B solution will produce strong radiative waves that will destroy the kicked solution and the overall transport.

IV. EFFECTIVE TRANSPORT

After studying the main properties of a set of six fundamental solutions, we look for conditions to observe mobility on a nonlinear Lieb lattice. The stability and Hamiltonian analysis give us information about the regions of parameters where a possible coherent mobility could be observed. For a very low level of power, the ring mode is weakly unstable, while the $2R$ mode is almost stable (there is a fluctuating regime for the stability of this mode, with values very close to zero, which implies an effectively stable propagation for typical propagation distances). When both modes bifurcate at $k_z = 0$, their effective area is quite similar, so there is no a clear distinction of solutions in terms of frequency, power, stability, and Hamiltonian. In fact, we found a clear Hamiltonian crossing close to $P \approx 0.95$ [see Fig. 3(b1)]. As this region looks promising for trying to observe coherent mobility, we numerically integrate model (1) considering a R mode as initial condition, with different input powers around $P = 1$. We integrate the dynamical equations on a lattice having 225 sites up to a given distance $z_{\max}$. As the R mode is a static stationary solution, we perturb it by applying an initial kick to its profile: $\psi_{\vec{n}}(0) = \psi_{\vec{n}}^R \exp(ik_y\vec{n})$, with k_y a horizontal wave vector and $\psi_{\vec{n}}^R$ the R-mode profile. This kick imprints a phase structure at the input condition, forcing the R mode to move on a horizontal direction. In order to characterize the mobility of ring modes on a Lieb nonlinear lattice, we made a sweep of parameters varying the input power in the interval $\{0, 2\}$ and k_y in the interval $\{0, 1\}$. Using the horizontal center of mass, defined as $Y(z) \equiv \sum y_n |\psi_{\vec{n}}(z)|^2 / P$, with y_n being the horizontal lattice position, we measure the propagated distance $d_y(z) \equiv |Y(z) - Y(0)|$. For a given set (k_y, P), we generate a set of distances d_y, in the interval $z \in \{0, z_{\max}\}$, and look for the largest value defined as $d_{\max}$. Figure 4, left collects our results, where we observe that for powers below $\approx$0.3, mobility is only marginal. Then, we do not observe a simple tendency and, in fact, we observe a rather chaotic dynamics, with large fluctuations for very close input conditions (this effect is also enhanced because $d_{\max}$ is measured at different distances). We observe some islands

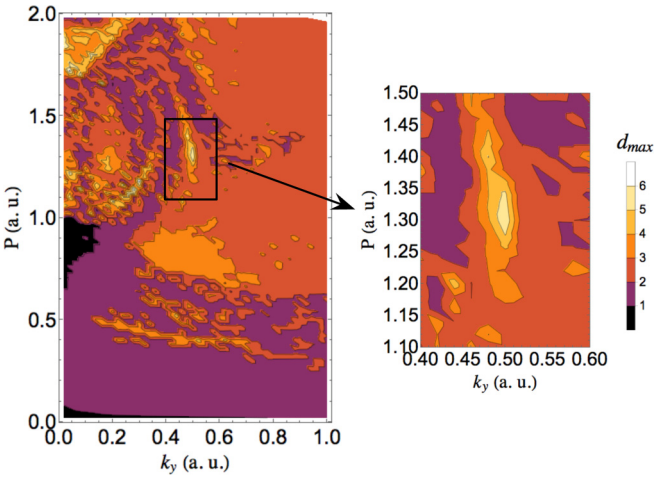

FIG. 4. $d_{\max}$ versus power P and horizontal kick k_y, for an R-mode input condition.

of enhanced mobility and we simply focus on the largest $d_{\max}$ values [see Fig. 4, right]. Around parameters $(k_y, P) \approx (0.5, 1.3)$, we find that the center-of-mass transport could be as much as a displacement of six sites. As the transport is occurring mainly in the horizontal direction, in Fig. 5(a) we plot the vertically integrated dynamics (i.e., we simply sum the intensity along the vertical direction) versus propagation distance z. We clearly observe that the ring profile is moving coherently, without the emission of noticeable radiation. The nonlinear R mode is able to jump four rings positions, moving

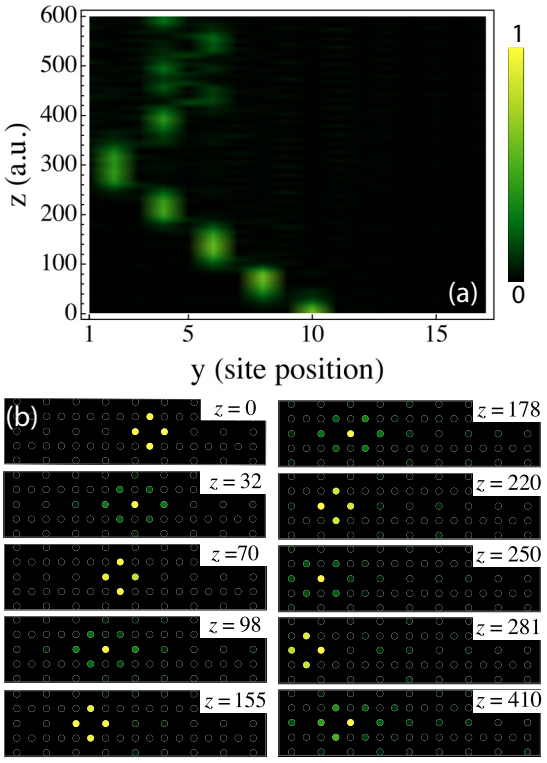

FIG. 5. (a) Vertically integrated intensity for an R-input condition at the bulk of a Lieb lattice. The input power is $P = 1.3$ with a horizontal kick of $k_y = 0.5$. (b) Intensity profiles at different z values.

its horizontal center of mass from position 10 to position 2 (the emitted radiation produces a larger effective ring translation than center-of-mass displacement). After reaching the lattice border, the profile is reflected back and tries to continue moving. However, we observe the emission of radiation and the consequently reduction of the power, what immediately changes the dynamical regime, stops the transport, and even destroys the ring profile. In Fig. 5(b) we directly show how this coherent transport is occurring. We clearly see that the ring profile is smoothly changing its form from a R mode at $z = 0$ to a $2R$ profile at $z = 32$, and then to a new R state at $z = 70$, located two sites away from the original profile. Then, as the figure shows, the coherent transport continues until the profile reaches the lattice edge. During the propagation, we do not observe neither a noticeable destruction of the profile nor a relevant reduction of power; so, we are in the presence of a very nice example of discrete coherent transport on a Lieb nonlinear photonic lattice. This transport is occurring for highly localized profiles and for very low level of power, which is an important aspect when considering the control of optical signals on a photonic device.

It is possible to think that an increment in the system size would imply a direct improvement in the transported distance; however, this is not necessarily the case due to the rather chaotic results presented in Fig. 4. The emitted radiation at the beginning and during the transport could generate a completely different dynamic, which depends very strongly on the input conditions. We repeated the numerical integration for lattices with different system sizes, and also considering different input positions. We found that every system has its own dynamical phenomenology, which is expected due to the rather chaotic behavior commented before. Multiple reflections on different surfaces could contribute to achieve an improved mobility or simply the opposite. When trying to move a localized stationary solution by adding a kick, we are forcing a static profile to move across the lattice. This always produces radiation of energy to the rest of the system that could enhance or diminish the effective mobility. The observed phenomenology strongly depends on the particular system size and specific input conditions.

Finally, we add a short comment about considering a binary Lieb lattice; i.e., a lattice having a binary profile for the propagation constant $\beta_{\vec{n}}$, such that the linear spectrum still includes a flat band (this is obtained by taking $\beta_A = \beta_C$, independent of β_B). We implemented this in order to study the effect of opening a gap of size $|\beta_A - \beta_B|$ in between the FB and the lower dispersive band. However, we find that the $2R$ mode gets unstable for even smaller powers; therefore, the multistability regime at low power is in fact reduced. Furthermore, we ran different sweeps such as the one shown in Fig. 4 and we did not find better mobility results compared to the ones presented above.

V. CONCLUSIONS

In conclusion, we studied the main properties of Lieb nonlinear photonic lattices. We focused on six different nonlinear stationary solutions to construct a dynamical picture for this lattice. We found that two of these solutions bifurcate exactly at zero power at the FB of the linear spectrum. The rest of the solutions follow a standard bifurcation process from an extended mode at the band edge. By analyzing the Hamiltonian and stability properties of these solutions, we conclude that there is only one regime for finding good mobility in this lattice, where the R and $2R$ modes posses effectively the same H value. This occurs for a low level of power, where these two modes are highly localized solutions. This is quite important when looking for concrete applications using photonic lattices, due to the goal of achieving good signal control at low level of power and, simultaneously, occupying a reduced spatial area. In addition to previous findings considering other FB lattices [23], our present results show that well-known standard properties of nonlinear cubic systems can dramatically change when nonconventional lattice geometries are considered.

ACKNOWLEDGMENTS

The authors want to thank D. López-González, L. Morales-Inostroza, P. P. Beličev, G. Glirorić, A. Maluckov, M. Stepić, and M. Johansson for fruitful discussions at the beginning of this work. The authors acknowledge financial support from Millennium Institute for Research in Optics (MIRO) and FONDECYT Grant No. 1151444.

[1] D. K. Cambpell, S. Flach, and Y. S. Kivshar, Phys. Today **57**, 43 (2004).
[2] F. Lederer, G. I. Stegeman, D. N. Christodoulides, G. Assanto, M. Segev, and Y. Silberberg, Phys. Rep. **463**, 1 (2008).
[3] S. Flach and A. Gorbach, Phys. Rep. **467**, 1 (2008).
[4] S. Deng, A. Simon, and J. Köhler, J. Solid State Chem. **176**, 412 (2003).
[5] S. Miyahara, K. Kubo, H. Ono, Y. Shimomura, and N. Furukawa, J. Phys. Soc. Jpn. **74**, 1918 (2005).
[6] D. L. Bergman, C. Wu, and L. Balents, Phys. Rev. B **78**, 125104 (2008).
[7] S. Flach, D. Leykam, J. D. Bodyfelt, P. Matthies, and A. S. Desyatnikov, Europhys. Lett. **105**, 30001 (2014).
[8] L. Morales-Inostroza and R. A. Vicencio, Phys. Rev. A **94**, 043831 (2016).
[9] D. Leykam, A. Andreanov, and S. Flach, Adv. Phys.: X **3**, 1473052 (2018); D. Leykam and S. Flach, APL Photonics **3**, 070901 (2018).
[10] R. A. Vicencio and C. Mejía-Cortés, J. Opt. **16**, 015706 (2014).
[11] R. A. Vicencio, C. Cantillano, L. Morales-Inostroza, B. Real, C. Mejía-Cortés, S. Weimann, A. Szameit, and M. I. Molina, Phys. Rev. Lett. **114**, 245503 (2015).
[12] S. Xia, Y. Hu, D. Song, Y. Zong, L. Tang, and Z. Chen, Opt. Lett. **41**, 1435 (2016).
[13] Y. Zong, S. Xia, L. Tang, D. Song, Y. Hu, Y. Pei, J. Su, Y. Li, and Z. Chen, Opt. Express **24**, 8877 (2016).
[14] B. Real, C. Cantillano, D. López-González, A. Szameit, M. Aono, M. Naruse, S. Kim, K. Wang, and R. A. Vicencio, Sci. Rep. **7**, 15085 (2017).

[15] E. Arévalo, Phys. Rev. Lett. **102**, 224102 (2009).
[16] Yu. S. Kivshar and M. L. Quiroga-Teixeiro, Phys. Rev. A **48**, 4750 (1993).
[17] R. A. Vicencio, M. I. Molina, and Y. S. Kivshar, Opt. Lett. **28**, 1942 (2003).
[18] R. A. Vicencio and M. Johansson, Phys. Rev. E **73**, 046602 (2006); U. Naether, R. A. Vicencio, and M. Johansson, *ibid.* **83**, 036601 (2011).
[19] U. Naether, R. A. Vicencio, and M. Stepić, Opt. Lett. **36**, 1467 (2011).
[20] C. Mejía-Cortés, R. A. Vicencio, and B. A. Malomed, Phys. Rev. E **88**, 052901 (2013).
[21] S. Rojas-Rojas, R. A. Vicencio, M. I. Molina, and F. Kh. Abdullaev, Phys. Rev. A **84**, 033621 (2011).
[22] S. Rojas-Rojas, U. Naether, A. Delgado, and R. A. Vicencio, Phys. Lett. A **380**, 3185 (2016).
[23] R. A. Vicencio and M. Johansson, Phys. Rev. A **87**, 061803(R) (2013).
[24] P. P. Beličev, G. Gligorić, A. Radosavljević, A. Maluckov, M. Stepić, R. A. Vicencio, and M. Johansson, Phys. Rev. E **92**, 052916 (2015).
[25] P. P. Beličev, G. Gligorić, A. Maluckov, M. Stepić, and M. Johansson, Phys. Rev. A **96**, 063838 (2017).
[26] J. He, Y.-X. Zhu, Y.-J. Wu, L.-F. Liu, Y. Liang, and S.-P. Kou, Phys. Rev. B **87**, 075126 (2013).
[27] S. Mukherjee, A. Spracklen, D. Choudhury, N. Goldman, P. Öhberg, E. Andersson, and R. R. Thomson, Phys. Rev. Lett. **114**, 245504 (2015).
[28] D. Guzmán-Silva, C. Mejía-Cortés, M. A. Bandres, M. C. Rechtsman, S. Weimann, S. Nolte, M. Segev, A. Szameit, and R. A. Vicencio, New J. Phys. **16**, 063061 (2014).
[29] P. G. Kevrekidis and V. V. Konotop, Phys. Rev. E **65**, 066614 (2002).
[30] P. G. Kevrekidis, V. V. Konotop, A. R. Bishop, and S. Takeno, J. Phys. A **35**, L641 (2002).
[31] C. Danieli, A. Maluckov, and S. Flach, Low Temp. Phys. **44**, 678 (2018).
[32] K. J. H. Law, A. Saxena, P. G. Kevrekidis, and A. R. Bishop, Phys. Rev. A **79**, 053818 (2009).
[33] S. Flach, K. Kladko, and R. S. MacKay, Phys. Rev. Lett. **78**, 1207 (1997).
[34] R. A. Vicencio and M. Johansson, Phys. Rev. A **79**, 065801 (2009).
[35] A. Khare, K. Ø. Rasmussen, M. R. Samuelsen, and A. Saxena, J. Phys. A **38**, 807 (2005).
[36] N. G. Vakhitov and A. A. Kolokolov, Izv. Vyssh. Uchebn. Zaved. Radiofiz. **16**, 1020 (1973) [Radiophys. Quantum Electron. **16**, 783 (1973)].